Natural Hazards Research 3 (2023) 395–407

Contents lists available at ScienceDirect

Natural Hazards Research

journal homepage: www.keaipublishing.com/en/journals/natural-hazards-research

Filling data gaps using citizen science for flood modeling in urbanized catchment of Akaki

Abel Negussie Alemu [a,b,c,*], Alemseged Tamiru Haile [a], Andrew B. Carr [e], Mark A. Trigg [e], Getahun Kebede Mengistie [c,d], Claire L. Walsh [f]

[a] International Water Management Institute (IWMI), P. O. Box 5689, Addis Ababa, Ethiopia
[b] Water Technology Institute, Arba Minch University, P.O. Box 21, Arba Minch, Ethiopia
[c] Africa Centre of Excellence for Water Management (ACEWM), Addis Ababa University, Addis Ababa, Ethiopia
[d] Addis Ababa Science and Technology University (AASTU), Addis Ababa, Ethiopia
[e] School of Civil Engineering, University of Leeds, LS2 9JT, UK
[f] School of Engineering, Newcastle University, Newcastle Upon Tyne, NE1 7RU, UK

ARTICLE INFO

Keywords:
Citizen science
Flood model
Sensitivity
HEC RAS
Akaki
Addis ababa

ABSTRACT

Identifying and understanding the value of citizen science to improve flood modeling is of importance to flood risk management. However, there are few studies that explore the value of citizen science data, with most studies focusing on evaluating the accuracy of the data. This research articulates the added value of citizen science data in flood modeling studies. During flood events, citizen scientists measured river water levels at selected sites along a main reach of the Big Akaki River in Addis Ababa, Ethiopia. They also provided information to estimate water discharge of the ungauged tributaries. The data acquired was used to force a one-dimensional (1D) HECRAS flood model, and to evaluate the model's sensitivity to inputs and parameters. Varying the downstream boundary condition caused a significant difference in the simulated water level (up to 3.5 km upstream of the downstream boundary site). Correcting the Digital Elevation Model and consideration of river tributary flows in the model simulation resulted in an underestimation of the observed stage by 0.08 m. The sensitivity analysis also showed that results were more sensitive to the Manning roughness values of the channel than that of the floodplain. Finally, this study identifies future flood modeling data collection priorities (e.g. flow data for the tributary). The flood modeling of the study area would not have been realized without the citizen science data.

1. Introduction

Citizen science is the participation of public volunteers in collaboration with professional researchers to collect data and monitor the environment around them (Montargil and Santos, 2017; Assumpção et al., 2018). In response to concerns of researchers on data quality, studies have focused on evaluating the accuracy of citizen science data (e.g. Strobl et al., 2019; Aceves-bueno et al., 2017). Studies that show added value of citizen science for solving real world problems are rare and mainly address rainfall and average conditions in river discharge (Paul et al., 2020). Even in a well-funded hydrological monitoring network scenario, citizens can provide additional valuable data to advance the study of floods (Pandeya et al., 2021). However, the impact and value of citizen science data for flood risk management has received increased research attention only recently (Ferri et al., 2020; Wolff et al., 2021).

Citizen scientists can provide a variety of datasets that can benefit flood studies. For instance, the review by Assumpção et al. (2018) shows Citizens can collect water level, flood extent, velocity of the water surface, precipitation, land cover, and river cross-sections. The main challenge described by the authors was integration of citizen data with other data sources (gauging and remote sensing). Another challenge is the adequacy of the volume of data collected by the citizens. Addressing such challenges requires measuring equipment that is accessible to a large number of citizens while enabling repeated measurements to be taken during a flood event. Smartphone devices that are equipped with a LIDAR sensor offer a viable option to measure river water level with good accuracy (Sermet et al., 2020), although, at present, the majority of citizens do not own smartphones with such technology. Similarly, Pandeya et al. (2021) used a low-cost Lidar-based sensor to monitor river water level by citizen scientists, which was tested for improving community-based flood

* Corresponding author. P.O. Box: 21, Arba Minch University, Arba Minch, Ethiopia.
E-mail address: nugussie2127@gmail.com (A.N. Alemu).

https://doi.org/10.1016/j.nhres.2023.05.002
Received 30 December 2022; Received in revised form 12 May 2023; Accepted 12 May 2023
Available online 13 May 2023

risk management. The authors reported that the river level data that was collected by the citizen scientists using the low-cost sensor matched well with government recorded data. The review by Sy et al. (2019) shows citizen science can provide complementary approaches and data to traditional approaches. Citizen scientists can collect basic data for flood hazard assessment (e.g., rainfall, discharge, topography, and land cover), key flood hazard characteristics (e.g. flood extent, water depth, flow velocity, and durations) and provide useful information in scenario development for flood risk management. This helps to bring increased spatial and temporal coverage of flood studies and improve knowledge in areas which are not well covered in the literature.

A few studies reported the applicability and limitations of citizen science data for flood modeling. In Rollason et al. (2018) , the flood data collected by the volunteers were the pathways of the flood (including area of overtopping and flow direction), impacts (maximum flood inundation extent), and timing of key flooding situations. Starkey et al. (2017) addressed the limitations associated with using citizen science to provide event information (duration, magnitude and intensity) for flood model calibration. They engaged citizens in the collection of both quantitative (e.g. daily rainfall amount) and qualitative data (e.g. starting and finishing time of the event). Observations during night-time hours are often difficult to acquire using citizen science approaches. Bannatyne et al. (2017) found that volunteers missed flood flow measurements occurring during night-time; although they were able to record flood wrack marks left on standing features. Loftis et al. (2019) validated a flood forecasting model by collecting the maximum flood extent and geotagged photographs using citizen scientists. Similarly, Fava et al. (2019) showed that citizen science data can be merged with traditional data to improve flood forecasts. The authors used the water level data recorded by citizen scientists to update real time flood forecasts at gauged and ungauged parts of a catchment.

In hydrodynamic flood modeling in ungauged basins, one of the major constraints is a lack of stream flow data to define the boundary conditions that drive the model, as well as calibration and validation of the model. Several studies have used different approaches to overcome this constraint but most of them did not explore the role of citizen science. For instance; Ruiz-bellet et al. (2017) used a critical depth type upstream boundary condition to reconstruct a historical flood event; whereas, Lamichhane and Sharma (2018) used peak-flow frequency statistics from regional regression equations developed for the USA (http://streamstats.usgs.gov). However, peak flow statistics alone do not provide the entire hydrograph of an event. This problem can be overcome by generating a synthetic triangular discharge hydrograph (Haile and Rientjes, 2007). Rainfall-runoff models also generate hydrographs for upstream boundary conditions (Ashok et al., 2018; Natarajan and Radhakrishnan, 2020). Many rainfall-runoff models rely on rainfall inputs which may not be readily available. Tedla et al. (2022) demonstrated that where coverage of the traditional rain gauge network is not adequate, citizen scientists can provide data with adequate quality and spatial coverage. The authors emphasized the need to consider attributes of the citizen scientists while training and supervising them during data collection.

Filling data gaps for calibration and validation of flood models has been a subject of previous research. Sanyal (2017) showed that information extracted from MODIS satellite images acquired during the peak of the flood events can be used to calibrate a flood model. However, MODIS images have a low resolution (>250 m) which does not provide detailed inundation patterns. This can be overcome with the use of Sentinel-1 images which have a 10 m resolution (e.g. Ezzine et al., 2020). Still, satellite observations require ground truthing for training the flood detection algorithms (Bekele et al., 2022). This provides another opportunity to engage citizen scientists in filling data gaps for flood studies although there are only a few published studies exploring this opportunity. An example is the study by Dasgupta et al. (2022) which showed that distributed flood water level data observed by citizen scientists can be used to calibrate a flood model.

The main aim of this study is to demonstrate the usefulness of citizen science for flood modeling, including an evaluation of model uncertainty through a sensitivity analysis of input data and parameters. Specifically, a 1D HEC-RAS model is used to simulate inundation on the floodplain of the Big Akaki River, situated in Addis Ababa, Ethiopia. Unlike many other studies (Muthusamy et al., 2021; Ferreira et al., 2021; Geravand et al., 2020), we evaluated the sensitivity of the model to several model inputs by: (i) integrating field measured cross-section data with the raw DEM, (ii) considering the effect of boundary conditions (tributary), and (iii) simulating the flood for a range of combinations of Manning's roughness coefficient of the river channel and floodplain. This study provides two main contributions. First, it demonstrates that citizen scientists can provide sub-hourly measurements of water levels if they are engaged properly. Second, the study shows the value of citizen science data in evaluating sensitivity of flood models, which is often not performed due to lack of data. In this study we explicitly assess the reliability of using citizen science data to calibrate flood simulation models for the prediction of water levels in rivers. The findings of this study are expected to increase research interest in the application of citizen science to evaluate the uncertainty of flood models.

2. Materials and methods

2.1. Study area description

The Akaki catchment is a tributary of the Awash River in the central part of Ethiopia. The catchment hosts Addis Ababa, the capital city of Ethiopia, and other small towns, which are rapidly growing. Specifically, the study area starts downstream of the confluence of Kebena and Bulbula Rivers and stretches along the Big Akaki River down to the boundary of Addis Ababa in the southerly direction (Fig. 1). Geographically, the study domain stretches from 8°50′42.2″ N to 8°56′24.32″ N and 38°44′ 30.1″ E to 38°50′ 0.73″ E. The domain has a river length of 18.1 km and a model extent that varies from 0.25 km to 5.3 km.

According to Bekele et al. (2022) the Akaki catchment is generally categorized into seven land use land cover classes (LULC): rainfed agriculture, built-up, bare land, forest area, grass land, irrigated and water body. The largest part of the catchment is covered by rainfed-agriculture (33.98%) and built-up areas (25.55%). According to Worako (2016) the LULC of the catchment at different times showed significant changes. The urban area coverage has increased at the expense of a reduction in agricultural land.

The Akaki catchment has a main wet season and a secondary one. The main wet season is called “Kiremt”, which occurs from June to September and contributes 70% of the total annual rainfall amount. The catchment experiences a second, less pronounced, seasonal increase in rainfall during the “Belg” season from mid-February to mid-April. The study area has an annual average rainfall of 1254 mm yr^{-1}, and the maximum monthly rainfall varies from 250 mm to 300 mm in July and August. The 25 year, 50 year, and 100 year return periods of daily total rainfall of Addis Ababa are estimated as 85.7 mm, 94.1 mm, and 102.4 mm respectively (Ethiopia Roads Authotity, 2013).

Previously, the Big Akaki River was monitored using automatic water level measurements around the new bridges on Addis Ababa to Adama Road starting from 1981, but these ceased in 2005 (Asfaw, 2007). The river has a mean annual flow of 274.3 $m^3\ s^{-1}$. The range of yearly maximum flows recorded from 1981 to 2004 varies from 36.5 $m^3\ s^{-1}$ to 693.1 $m^3\ s^{-1}$. The largest flow was recorded in August 1999. However, the automatic recorder came out of service in 2005. Currently, an observer is collecting the water level manually twice per day. We observed in the field that the staff gauge is repeatedly damaged by floods.

2.2. Data sets

In this study, primary data (field data) and secondary data (from global and national archives) were collected to serve as inputs to the

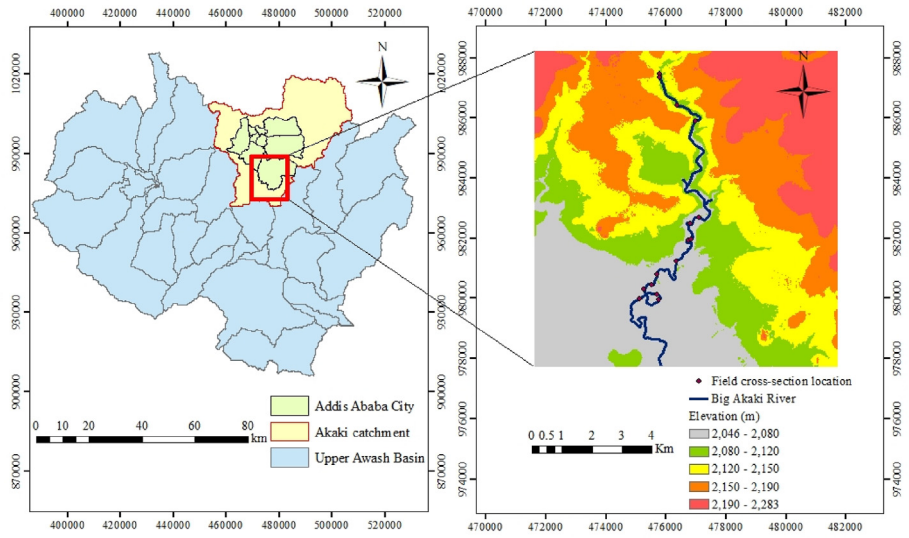

Fig. 1. Geographic setting and elevation variation of the study area.

flood model. Citizen scientists who volunteered to collect river water level data were first identified through a face-to-face meeting between community members and the research team. The main criteria for selecting a citizen scientist was the ability to read and write in the local language. Next, training was provided to the citizen scientists on the use of the measurement instruments and using the data recording sheet. Simple instruments were used for the water level measurement. Since the measurements were taken beneath bridges, citizen scientists were provided with a rope, stick and measuring tape to measure the distance between the top of a bridge and the water level. Using the river cross-section data also acquired in this study, we were able to convert the citizen science data to river water depth. The water level measurements were taken during heavy rainfall events in the upstream parts of the catchment. They conducted the measurements over the duration of each selected event at 15–30 min time interval, depending on the rate of change of the water level.

Those events that started early in the morning or lasted beyond 19:00 h were not measured as it was not safe for the citizen scientists to stay at the measuring site. As a result, they captured data of only a few, but very important, events that can help understand the flood characteristics of the area and set-up of a flood model of the study area. Nine events were captured in 2020 and four events were captured in 2021. However, only four of the events (September 04, 2020; July 10, 2021; July 17, 2021 and September 08, 2021 that have maximum water depth at Akaki bridge 5.15 m, 3.18 m, 3.10, and 5.35 m respectively) were found useful for further analysis, as the water level data was concurrently captured for the entire duration of the events at multiple sites. However, if we considered those events that were not concurrently captured for the entire duration as official historical flood, we should go back to the field and use different method of hydraulic measurements for obtaining the flow and other hydraulic parameters. This can be supported with observation of the flood marks and consultation of the community.

The water level measurements were converted to flow rate data by developing rating curves at measuring sites (upstream of study area and Akaki new bridge). A rating curve was developed by using a power law function. The calibration parameter was estimated by using nonlinear least square methods; the rating paired measurements of depth and velocity is converted to discharge using river cross-sections (continuity equation). In this study uncertainty analysis on the water level measurements recorded during the rainfall events is carried out at two stations. The error metrics that we applied are mean absolute percentage error (MAPE), mean absolute error (MAE), and root mean square error (RMSE).

The digital elevation model (DEM) is one of the most important datasets for flood modeling as it represents the geometry of the channel and floodplain. In this study, a 5 m resolution DEM was obtained from the Ethiopian Geospatial Information Institute (EGII). The DEM was developed using photogrammetry in 2017 with an object point of 0.02 m plan metric and 0.04 m height. In this study, off-terrain objects (e.g. houses) were not removed from the DEM as these were scattered and considered not to create big issue in the model domain.

The field data collection involved river cross-section surveys. This entailed measurement of paired horizontal coordinates and the depth to the channel bed to describe the river cross-section geometry perpendicular to the river channel. Horizontal coordinates were recorded using a combination of handheld global positioning system which typically have a ± 3 m horizontal accuracy and measuring tape. The beginning and end points of the cross-section were geolocated and the intermediate points' positions were recorded from the (more accurate) tape measure distance. A measuring tape of 30 m was stretched between two reference stakes on top of the two banks of the river channel. The horizontal distance was measured along with the stretched measuring tape whereas depth was measured from the measuring tape to the channel bed. A spirit level was used to maintain consistent levels along the vertical and horizontal of each measurement site. For this study, 15 river cross-sections were measured before the rainy season of 2020. The cross-section interval along the river ranged from 0.25 km to 2.2 km depending on the variation in cross-sectional channel geometry and site accessibility. The citizen scientists supported the cross-section survey.

Locations of cross-sections can have a very significant effect on flood modeling. In this study, a set of criteria were identified and followed to select the measurement location of cross-sections. First, the measurements were taken where there is a change in river channel or floodplain geometry (width, depth, and roughness of the channel and floodplains). Secondly, cross-sections were measured at bridges where there is significant obstruction of river flow. Finally, accessibility of the site for measurement was considered.

Manning's roughness coefficient (n) represents a surface's resistance to water flow in the channel and floodplain. Estimation of its value requires information on land cover, channel bed conditions, and channel alignment. During the field survey, photos of the channel bed material, channel alignment, and land cover were captured. Since the photos of the channel bed material was invisible during the flood season, photos were taken during dry periods where most parts of the channel bed were dry due to low flow conditions. However, parts of the riverbed were not visible at some sites because they remained submerged. For those sites,

we took grab samples of the bed material and compared it against standard photos of features with known roughness. For the river channel, the photos were compared against standard photos of features with known roughness to estimate the roughness based on tabulated values in hydraulics books of Chow (1959) and Arcement and Schneider (1989).

An LULC map was used to estimate flooded areas under different land classes and to assign Manning roughness values for the floodplain. The LULC was prepared by Bekele et al. (2022) using Sentinel-2 images. Road data was used to estimate flood affected road types and length. The road data of the study area was collected from freely available OpenStreetMap data using the BBBike Extract Service (https://extract.bbbike.org/). To determine the length of flood affected road types, the flood map was intersected with the road types using an overlay analysis in Arc GIS.

To simulate hydrodynamics, HEC-RAS requires specification of initial conditions along with upstream and downstream boundary conditions. The water level measurements acquired by citizen scientists provided an upstream boundary condition. Specifically, stage data at the upstream boundary was measured for many days during the rainy season of 2020. It was difficult to capture event peaks since the peaks repeatedly occurred during night, which was an unsafe time for the observers to be at the measuring site. However, the rising and falling limbs of the stage hydrographs and the peak were captured on September 04, 2020 and hence the stage hydrograph data of this date served as the boundary condition. In addition, the water level of the same event was measured at the middle part of the model domain and served as reference data for evaluation of the simulated water levels.

2.3. Methodology

2.3.1. Integrating field measured cross-section data with DEM

In this study, a 5 m resolution DEM was used, which was found to have some limitations in accurately capturing the bathymetry below the water level. Considering the river width is not large (mostly <40 m), the 5-m DEM may smooth the riverbed elevation missing important details. As a result, it was found necessary to correct the DEM using field data of the channel cross-section. Before integrating the raw DEM data and field cross-section data, it was necessary to match the spatial reference system of the DEM and field-collected cross-sections. The DEM which was collected from the Geospatial Information Institute (GII) was prepared using Adindan coordinate system (projected coordinate system for Ethiopia, Eritrea and Sudan) whereas field data was collected using the WGS84 UTM zone 37 N coordinate system. Hence, the coordinate system of the DEM was converted to WGS84 UTM zone 37 N coordinate system. Fig. 2a shows that noticeable difference between the maximum depth and shape of the channel cross-sections obtained from the DEM and field survey. Hence it was not possible to perfectly correct all aspects of the cross-section, but the corrected cross-section is still acceptable to serve as the model input. In Fig. 2b, there is similarity between the shape, width, and depth of the cross-sections from the two sources. The main difference between the two cross-sections was a horizontal shift. Therefore, we were able to perfectly correct the cross-section to the extent that the difference between the corrected and field cross-sections is not visible.

One of the main challenges in flood modeling is the inability of the terrain data to capture the riverbed elevation. In this case modification or correction of the terrain data is needed and we used the method commonly known as “burning the channel into the DEM”. In this study, the RAS Mapper tool was used to modify the original DEM data using our field elevation data that was measured using a simple technique (GPS, rope and measuring tape) with 1 cm accuracy. For the DEM modification, RAS Mapper is an interface that is used to process geospatial data and allow modification of geometric data and visualization of HEC-RAS simulation results. RAS Mapper has the ability to create new terrain using cross-section data from the HEC-RAS model and from interpolated surface cross-section sub layers (Brunner, 2016). To obtain the corrected cross-section at selected sections, the original cross-section from the DEM was first corrected with our field collected cross-section in MS excel. The RAS terrain tool was used to integrate the corrected cross-section at selected sites with the entire DEM. The integration technique uses the shape, depth, and width of cross-section as input for matching. First, the width of the two datasets was matched by correcting the DEM channel depth either on the left or right side (Fig. 2). This is followed by matching the channel depth from the two datasets at the other parts of the cross-section. Finally, the three cross-section plots (uncorrected, field and corrected) were compared to visually inspect the results of the cross-section integration (Fig. 2).

2.4. HEC-RAS model

HEC-GeoRAS 10.4 is an auxiliary ArcGIS tool to HEC RAS and it is used for the processing of geospatial data and analysis of water surface profile results. In this study, it was used to extract geometric data like river centerline, banks of the river, the flow path of the river, and cross-section cut lines as required for input to the HEC-RAS model. The left and right banks and center lines of the river were digitized in Google Earth and imported to Arc-GIS for projection, to aid the preprocessing and preparation of input data of the model. For further analysis, the coordinate system of the digitized data was transformed to WGS84 UTM zone 37 N coordinate system. Finally, the extracted cross-sectional data was exported to HEC-RAS as a model input to simulate flooding (Fig. 3).

In this study, HEC-RAS was used to simulate river and floodplain hydrodynamics. The one-dimensional (1D) module of the HEC-RAS model computes water surface elevation for each cross-section cut line by solving the flow governing equation of momentum and mass conservation (Kane et al., 2017). The main inputs of the HEC-RAS model are river and flood geometric data, Manning's roughness coefficient ‘n’ value for the river and the floodplain area, upstream and downstream boundary conditions, and initial conditions. A stage hydrograph was used for the upstream boundary condition, and a normal depth or friction slope (value of 0.01) was specified for the downstream boundary condition after sensitivity analysis. The event water level data that was observed on September 4, 2020 served as the upstream boundary condition for actual simulation of the main river. The simulation period has a length of 24 h

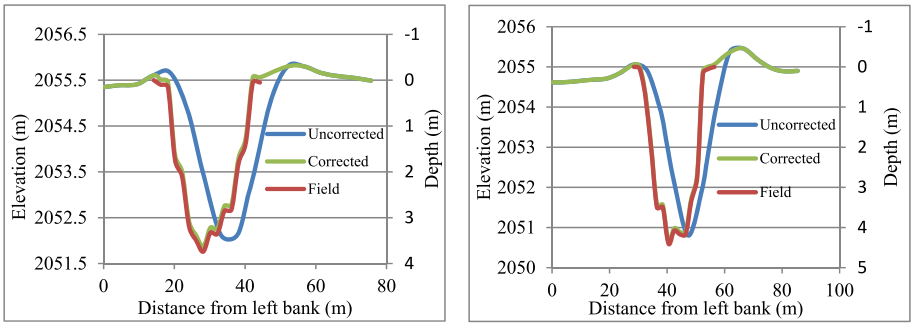

Fig. 2. The river cross-section profile at different location for the uncorrected, field and corrected DEM.

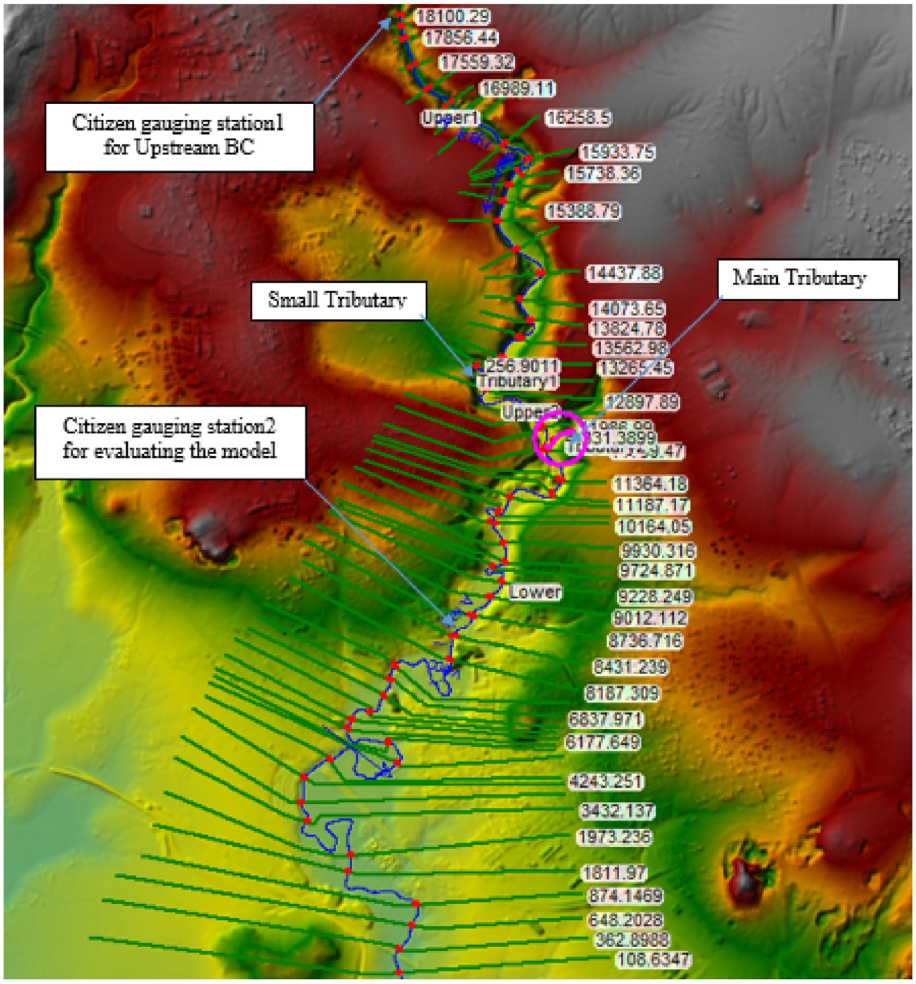

Fig. 3. Schematic view of the pseudo-3D terrain model of the study area with cross-section cutline.

stretching from 00:00 to 24:00 h.

HEC-RAS requires initialization to capture the water level before the actual simulation period. The model can be unstable for poorly defined initial condition data (Brunner, 2016). In this study, a one-week period (from August 28, 2020 to September 03, 2020) was used for initializing the HEC-RAS model of the study area. Twice per day measurements of water levels for model initialization were conducted with the engagement of citizen scientists.

2.5. Model evaluation criteria

Mean absolute deviation (MAD), mean square error (MSE), and root mean square error (RMSE) were used to evaluate the accuracy of the simulated water level. According to Lee et al. (2018), these accuracy measurements are appropriate since they show errors in the units or square error of the component of interest. Zero values of MAD, MSE, and RMSE indicate that the observed and simulated water levels show a perfect fit. In reverse, large values of these criteria show large mismatches between the observed and simulated water levels. The equations of the criteria reads as follows:

$$MAD = \frac{1}{n}\sum_{i=1}^{n} abs(WL_{i,sim} - WL_{i,obs}) \quad (1)$$

$$MSE = \frac{1}{n}\sum_{i=1}^{n} (WL_{i,sim} - WL_{i,obs})^2 \quad (2)$$

$$RMSE = \sqrt{1 \Big/ n \sum_{i=1}^{n} (WL_{i,sim} - WL_{i,obs})^2} \quad (3)$$

where: *WL* refers to the water level (m), the subscript *i* indicates time step, the subscripts *sim* and *obs* indicate simulated and observed quantities respectively and *n* refers to the total sample size.

2.6. Assessment of model uncertainty using sensitivity analyses

The sensitivity analyses included an analysis of the effect of model inputs, tributaries, parameters, and boundary conditions. This required a total of 41 model runs (Table 1). Most of the model runs were conducted to test the model sensitivity to its main parameter which is the Manning roughness coefficient.

First, the flood model was developed by using cross-sections from the original raw DEM without any corrections. Then, the model was set up for the cross-sections which were extracted from the DEM and corrected using the field-collected cross-section data. Finally, the simulated water

Table 1
Summary table on the number of tests or model runs.

No.	Type of model uncertainity test	No. Of runs in each tests
1.	Crosssection correction	2
2.	River tributaries	2
3.	Manning roughness	32
4.	Downstream BC	5

levels for the two conditions were graphically presented for comparison (Fig. 5a).

Further sensitivity tests were conducted to evaluate the effect of inflows from two minor tributaries on the flood simulation. The effect of stream flow of tributaries on flood simulation was assessed by setting up the flood model for three situations. First, the model was set up only for the upstream boundary condition without considering tributaries. Next, the model was set up for the upstream boundary condition and specifying a boundary condition for the larger tributary. Finally, both tributaries and the upstream boundary conditions were considered in the model.

For the tributary rivers, a discharge hydrograph was developed based on community consultation and measurement of channel cross-section and velocity. Selected community members (residents) were consulted to estimate the maximum water level and wetted cross-section. Then we measured the river width and depth at different locations of the cross-section. Velocity was measured for normal flows during our field visit, and was extrapolated based on our own experience of measuring velocity of peak flow in other gauging sites in the same river. The aim of our study is to evaluate the sensitivity of the model's response to inputs. However, future studies that aim to map the actual flooding map should measure the actual velocity at a range of water levels. To estimate the discharge (upstream boundary condition of the tributaries), the measured river cross-section was multiplied with the velocity. Maximum flows of 39.8 m^3/s and 10.04 m^3/s were estimated based on the wetted cross-section for the maximum water level and flow velocity for tributary 1 and tributary 2 rivers respectively, by assuming a channel velocity of 1 m/s. This translates to 10.13 and 40.15% of the peak stream flow at the upstream boundary site as observed by the citizen scientist on September 04, 2020. In addition, to calculate the minimum or base flow for the tributaries, field observations of the river flow were acquired. These observations yielded minimum flow estimates of 1.01 m^3/s and 1.04 m^3/s for tributary 1 and tributary 2, respectively. The significance of the flood contribution of the tributaries was then evaluated by comparing the simulated water levels with and without including the tributaries (Fig. 5b).

The effect of Manning's roughness coefficient on flood simulation was evaluated with four cases. The first case involved fixing the roughness value in the floodplains but changing the roughness value in the channel section. For cases 2 and 3, the roughness values of the left and right floodplains were changed respectively while keeping the roughness of the channel constant. Finally, roughness values of both the channel and floodplains were changed simultaneously. The reference Manning's values that were adopted for this study are presented in Table 2.

The effect of boundary condition uncertainty was minimized by locating the model downstream boundary far away from the area of interest. In addition, different downstream boundary conditions were compared to assess sensitivity to the uncertainty: normal depth using friction slope, normal depth at 900 m distance from the actual downstream end of the model domain, and constant water level at 2052, 2053, and 2053.5 m at the downstream end. The main objective was to investigate how far the effect of uncertain boundary conditions propagates upstream along the channel so as to avoid the extra cost of measuring flows at the downstream end of the model domain. In this study, the channel at the downstream section has small conveyance capacity which results in frequent water overflow that makes flow measurement difficult.

3. Results and discussion

3.1. Base line model result

The maximum flood depth and extent map for the baseline model of the study domain was simulated by considering two river tributaries and cross-sections from the corrected DEM (Fig. 4). The study area has a 90th percentile flood depth and flood extent (area affected by flood) of 9.21 m and 2.95 km^2 respectively. The flood has high depth near the river channel and when it overflows upstream of the Akaki bridge. There is a very distinct difference between the flood depth and pattern upstream and downstream of the Akaki Bridge. The area downstream of the Akaki Bridge has a relatively widespread flood extent which has relatively small depth as compared to the upstream area. However, the flood depth is large enough to cause serious damage to people and property.

3.2. Effect of cross-section correction on simulated hydrograph

In this study, we first evaluated the effect of integrating channel cross-sections from a high-resolution DEM and field survey. The observed and simulated stage hydrographs are presented in Fig. 5a for comparison using September 4, 2020 event water level data. The overall pattern of the observed hydrograph is captured by the model by using the cross-section from the DEM and corrected DEM and field data. The slopes of the observed rising and falling limbs are satisfactorily captured. However, there are two major mismatches between the observed and simulated hydrographs (i) a large mismatch between the peak magnitudes, and (ii) a mismatch between times to peak.

The peak of the simulated stage for the raw DEM and corrected DEM are 2060.94 m and 2061.52 m respectively. This shows a large underestimation of the observed stage (2062.49 m) by 1.55 m and 0.97 m for the raw and corrected DEM, respectively. Hence, integrating field-collected cross-section data in the original cross-section data from the DEM results in a significant improvement in the model performance. Here, unlike the study of Muthusamy et al. (2021), the correction of the DEM with cross-section data led to increased inundation area. This is because of the difference in data collection time of the raw DEM and field cross-section data. The DEM was generated in 2017 whereas the field data was collected in 2019. During this time interval, the Akaki River has undergone rapid changes due to sedimentation and erosion in addition to other human interference e.g. there is a crusher site that dumps materials into the river; and there is ongoing construction of a bridge upstream of this site that is disturbing the channel cross-section. The time of the peak flow for both the raw DEM and corrected DEM model simulations was 11:00 h, but the peak was observed at 08:50 h. These results imply that the simulated time of the peak is delayed by 2:10 h for both the raw and corrected DEM, and that the channel and floodplain storage capacity has significantly changed since the DEM was generated, indicating the importance of correcting the cross-section data.

3.3. Effect of river tributaries on stage hydrograph

The HEC-RAS model of the study domain was run by considering two selected river tributaries using the corrected cross-section DEM version of the model. The two tributaries have a total watershed area of 31.11 km^2. For comparison, the observed and simulated stage hydrographs are presented in Fig. 5b. The overall pattern of the observed hydrograph is captured by the model. The slopes of the observed rising and falling limbs are well captured.

Fig. 5b shows slight differences in the simulated peak flow magnitude when one and two tributaries were considered. The peak of the simulated stage is 2062.33 m and 2062.41 m when considering the contribution of one tributary (the larger tributary) and two tributaries, respectively. This shows a small underestimation of the observed stage by 0.16 m and 0.08 m respectively. As discussed previously (Section 3.2), specifying the boundary condition only at the major river and using the corrected DEM underestimated the observed peak by 0.95 m. This indicates consideration of river tributaries in the model simulation results in a reduction of the difference in the observed and simulated peak river stages. However, the results show that only the larger of the two tributaries needs to be monitored for a significant improvement in accuracy to be realized, which is pertinent in the context of budgetary constraints. The time of the peak flow was not changed by considering any of the tributaries.

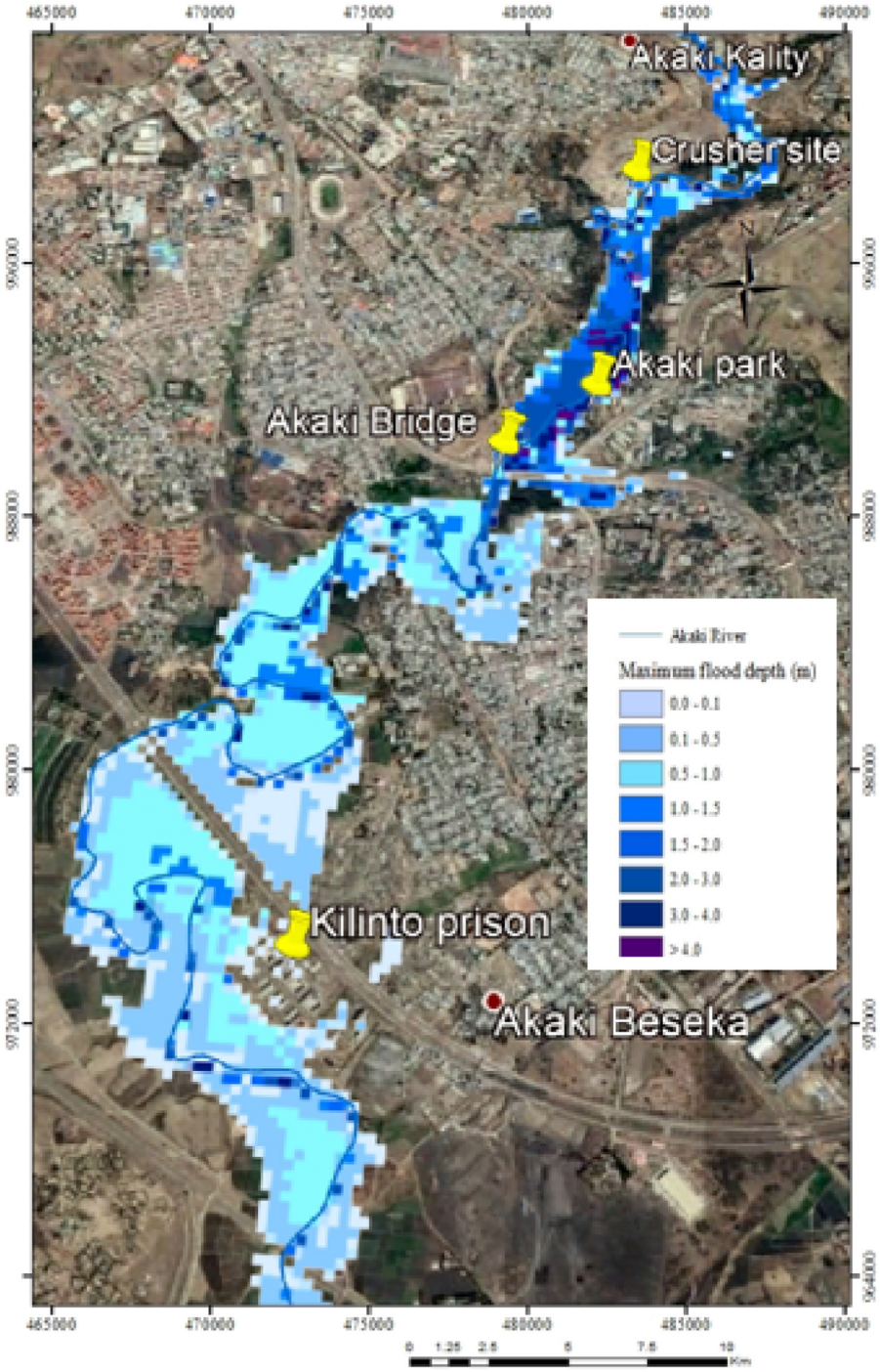

Fig. 4. Baseline model result of flood depth and extent.

3.4. Sensitivity to Manning's roughness values

The effect of Manning's roughness coefficient on flood simulation was evaluated with four cases. First, we ran the model by adding and subtracting various values to the reference Manning's value. The results of the preliminary model run showed that some level of sensitivity to increments/decrements of the Manning roughness by 0.004. This interval was also selected since it is smaller than the difference in Manning roughness values of various land cover classes. For illustration, Fig. 6 shows some hydrograph plots of the model run using the reference surface roughness, adding 0.004, and subtracting 0.004 from reference Manning's value of channel and floodplains. Increasing Manning roughness values by 0.004 resulted in underestimation of water level data by 1.53 m. It also resulted in earlier occurrence of the peak (i.e. 1:00 h earlier than the reference time of the peak). In contrast, subtracting 0.004 from the Manning's reference value resulted in overestimation of water level by 1.34 m and delay of time of peak by 1:00 as compared to the reference time of the peak.

In Fig. 7, the results of the sensitivity analysis are presented in terms of RMSE of the simulated water level as compared to the reference water level. The first case is by using the reference roughness value in the floodplains but changing the roughness value in the channel section (referred to 'channel' in Fig. 7). In this case, the RMSE rapidly increased when the roughness value was increased. The increment of the RMSE

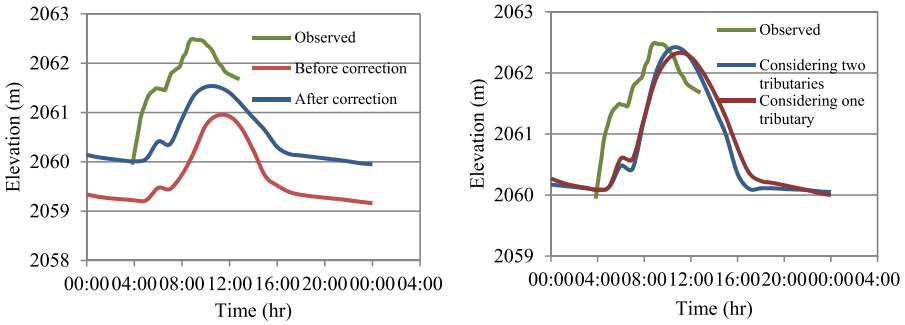

Fig. 5. (A) Effect of cross-section correction on the simulated stage (water level) hydrograph **(b)** Effect of considering river tributary on stage hydrograph.

Table 2
Reference Manning's roughness values for the channel and floodplain.

No	Type of river material and LULC	Manning's roughness value (n)
1	Cobbles with large boulders	0.05
2	Gravels, cobbles, and few boulders	0.04
3	Gravel	0.035
4	Coarse sand	0.031
5	Firm soil	0.0285
6	Bare land	0.03
7	Agricultural land	0.035
8	Forest Land	0.2
9	Grass- Land	0.035
10	Urban Land	0.11
11	Irrigated land	0.035
12	Water body	0.03

reached up to 1.32 m showing large deviation from the RMSE using the reference roughness, i.e. 0.72 m. This result implies that the simulated water level is highly sensitive to the roughness of the channel section.

For cases 2 and 3, the roughness values of the left and right floodplains were changed respectively while keeping the roughness constant for the channel and one of the floodplains (referred to 'left and right' in Fig. 7). Fig. 7 shows that the simulated flood level was not significantly sensitive to the roughness of the floodplains. In case 4, the roughness of the channel and floodplains was changed simultaneously (referred to 'All' in Fig. 7), the maximum RMSE was 1.32 m indicating a large deviation from the RMSE when changing the channel roughness, i.e. 0.72 m. This indicated that the effect of the floodplain roughness is relatively small at least for the considered river reach and flood event. Our finding is similar to that of Lamichhane and Sharma (2018) and Haile and Rientjes (2007) who reported that the simulated flood extent and water level are more sensitive to the Manning's roughness values of the channel than those of the floodplain.

3.5. Sensitivity to the downstream boundary condition

The result shows the effect of the downstream boundary condition appears only near the downstream end of the river and it disappears at 3.5 km upstream of the downstream boundary (Fig. 8). Hence, the simulated flood characteristics within this distance were not used for further analysis. Though not used in this study, it was also possible to extend the model domain with artificial river reaches (e.g. as copy of the final stretch of the river). Here, the constant water level causes higher water depth at the downstream end than the other boundary conditions. Whereas, specifying a normal depth at 900 m upstream from the downstream end causes lower water depth than that of other boundary conditions. The large difference in water level due to the remaining three downstream boundary conditions was sustained only up to 1.5 km

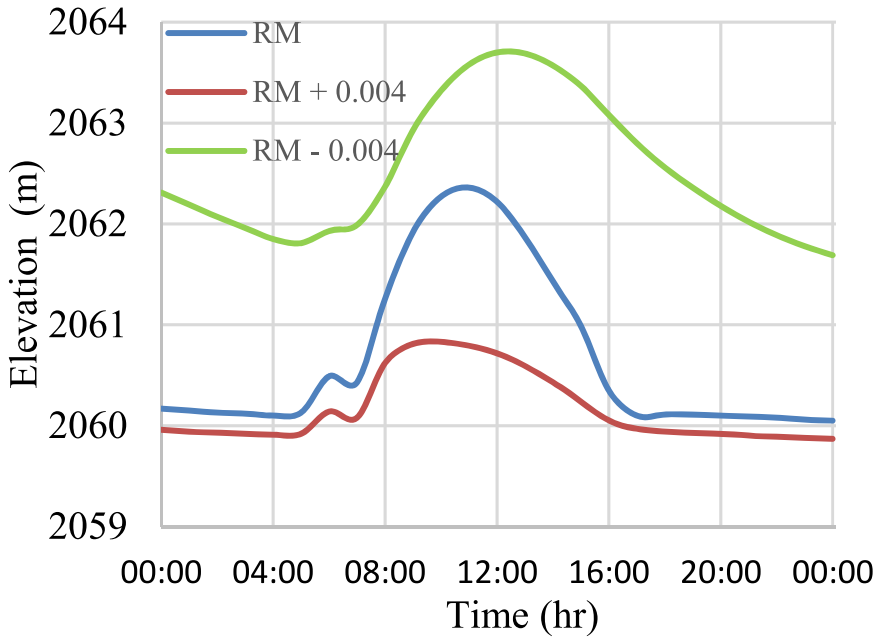

Fig. 6. Hydrograph plot for RM (Reference Manning's value) and some of the extreme values tested.

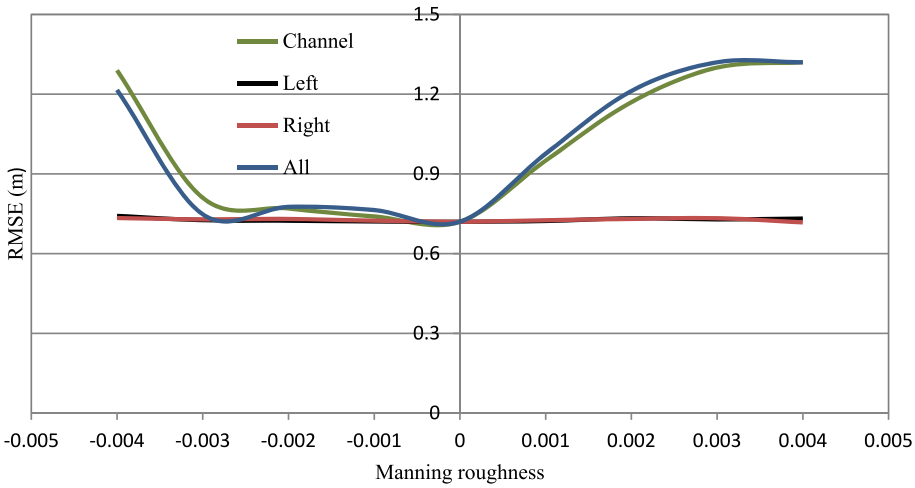

Fig. 7. Sensitivity of the model simulated water level in terms of RMSE by 4 cases of Manning's roughness values of the floodplain and river channel.

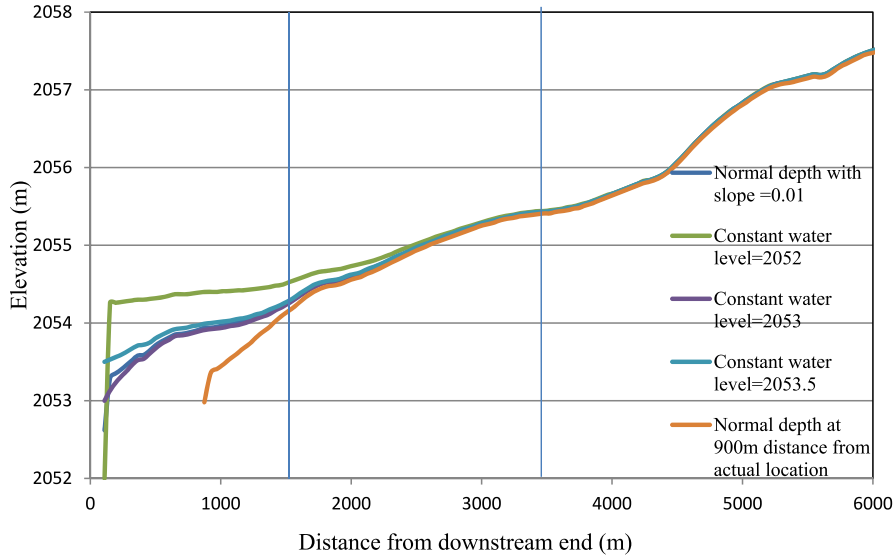

Fig. 8. Effect of various downstream boundary conditions on the simulated water level.

upstream of the downstream boundary of the model domain.

3.6. Attenuation and translation of the observed hydrograph

The flow hydrographs based on citizen science data were compared for two sites on the Big Akaki River (Fig. 9). These sites are situated downstream of the confluence of the Bulbula and Akaki Rivers (i.e. upstream of the studied river reach) and at the new bridge on the Akaki near Tirunesh Beijing hospital. In terms of pattern, the hydrographs at the two sites are somewhat similar. However, the hydrographs at the two sites have a mismatch in terms of peak flow due to attenuation effects. The peak flow was attenuated by 100.45 $m^3 s^{-1}$ and 64.93 $m^3 s^{-1}$ over the 9.7 km distance between the two sites on September 09, 2020 and July 17, 2021, respectively. Time to peak also shows a translation: the hydrograph was translated by 35 min and 70 min on September 09, 2020 and July 17, 2021 respectively.

The error statistics result for the rating curves at two stations are presented below in Table 3 below. The mean absolute percentage error (MAPE) for the Akaki new Bridge station and the Worku village station are 12.09% and 29.22% respectively. This implies the Worku village station (the station at upstream boundary condition) is more likely to have a high percentage error than the Akaki new bridge stations. In addition, stage discharge relationships derived from measured values are presented in Fig. 10 below. The Worku village station measurements show greater deviation from the derived rating curve than the Akaki new Bridge station measurements. Note this error does not have an effect in this study since stage data was specified as an upstream boundary condition.

3.7. Objective evaluation of the simulated water level

Table 4 summarizes the error statistics for model simulations using different DEM and tributary combinations. The mean absolute deviation from the observed water level was large (1.65 m) when the uncorrected DEM was used and the contribution of the tributaries was not considered. This significantly reduced to 0.84 m when the DEM was corrected using field measured cross-section data and dropped to 0.36 m when the contribution of one tributary was considered. Considering the second tributary had little effect on mean absolute error (there was actually a small increase in MAE). From all combinations, consideration of one

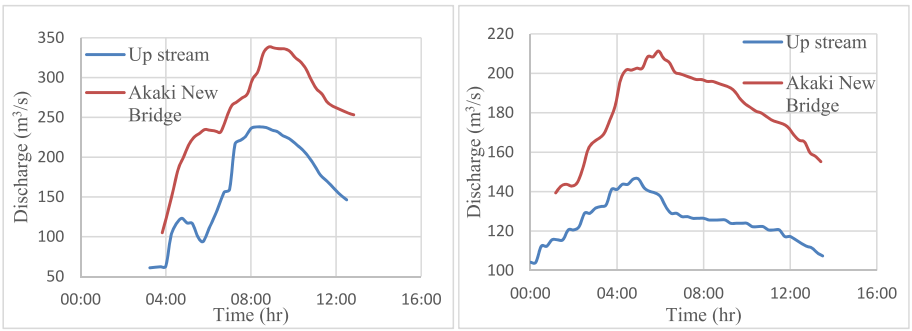

a. Flow hydrograph for September 09, 2020 b. Flow hydrograph for July17, 2021

Fig. 9. Attenuation and translation of observed hydrograph in different seasons.

Table-3
Error statistics for Rating curve at two stations.

Error type	Akaki new Bridge station	Worku village station
Mean absolute percentage error (MAPE)	12.09	29.22
Mean absolute error (MAE)	3.55	5.07
Root mean square error (RMSE)	7.45	8.22

tributary combined with the corrected cross-section input produces the smallest mean square error (MSE) and root mean square error (RMSE) of 0.48 m and 0.69 m respectively. The uncorrected DEM (without considering the tributaries) has a very high MSE and RMSE of 3.05 and 1.75 respectively. We note that the smallest mean absolute deviation (0.36 m) is still a considerable magnitude, as it may cause significant loss of life and property damage.

3.8. Flood map

Table 5 shows the summary of simulated flood extent in the model domain for different DEM and tributary information. We find that the inundation area increased when the DEM was corrected for the channel cross-sections and the tributaries were considered. For example, the simulation using the uncorrected DEM results in the smallest flood inundation extent (2.74 km^2) whereas consideration of the two tributaries has the highest flood extent (2.95 km^2). Overall, the difference of the input data source results in up to 0.21 km^2 difference in the simulated flood extent.

Fig. 11 shows the inundation areas under each flood depth class for each input condition. The effect of the input data source is very distinct for flood depths less than 1.5 m. For low flood depths (<1.5 m), the uncorrected DEM resulted in a larger flood extent, which decreased as

Table 4
Summary of the error statistic for different model inputs.

Error Type (MAD, MSE & RMSE)	Mean absolute deviation (m)	Mean square error (m^2)	Root mean square error (m)
Uncorrected DEM	1.65	3.05	1.75
Corrected DEM	0.84	0.86	0.93
Corrected DEM by considering one tributary	0.36	0.48	0.69
Corrected DEM by considering two tributaries	0.43	0.50	0.72

Table 5
Summary of flooding map output as DEM and tributary information changes.

Flooding map output	Flood extent (area) km^2
Uncorrected DEM	2.74
Corrected DEM	2.87
Corrected DEM by considering one tributary	2.91
Corrected DEM by considering two tributary	2.95

corrections were added to the DEM and tributary information was added. For high flood depths, the uncorrected DEM resulted in the smallest flood extent. Most of the inundated area of the study area falls in the flood depth class of 1.0 m–1.5 m. The first flood depth class (0.0 m–0.1 m) has the smallest flooded area of all flood depth classes. In addition, flood depth classes less than 2 m (i.e. 0.0 m–2.0 m) constitutes 66.7% of the total inundated area. All flood depth classes less than 3 m (i.e. 0.0 m–3.0 m) constitutes 81.3% of the total inundated area.

In this study, land cover was overlaid (intersected) with the flood map to determine the extent or area of affected land cover type. Table 6 shows the inundated area of different land cover classes. The irrigated, grass

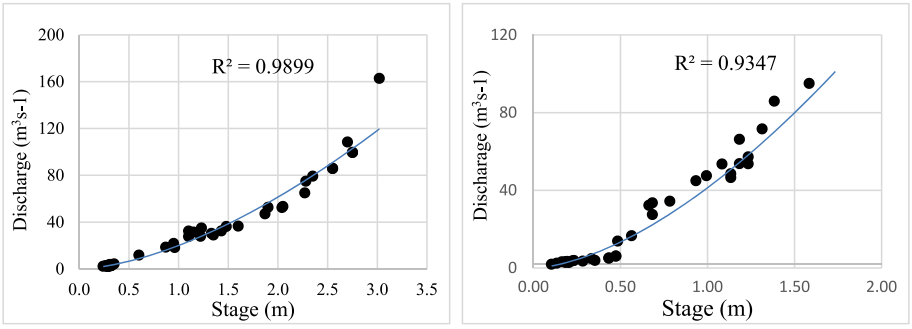

Fig. 10. Rating curve for Akaki New Bridge (left) station Worku village station (right).

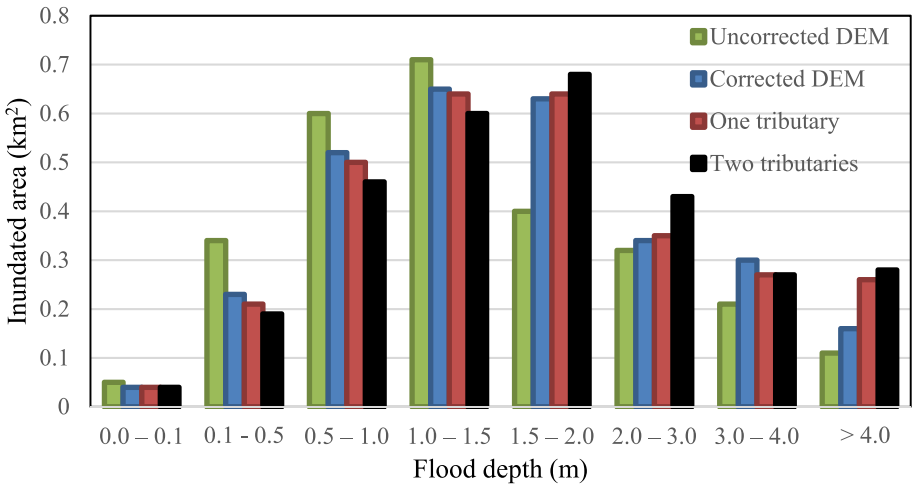

Fig. 11. Summaries of inundated areas (km^2) under each flood depth class.

Table 6
Flooding map area under different land cover type.

No.	Land cover type	Inundated area (km^2)	Inundated area (%)
1	Forest	0.332	11.26
2	Bare land	0.147	4.97
3	Grass land	0.345	11.70
4	Irrigated	1.531	51.90
5	Rain fed	0.260	8.81
6	Urban	0.327	11.08
7	Water body	0.008	0.28

Table 7
Length of road inundated, split by road type.

No.	Road Type	Length (m)
1.	Primary	66.74
2.	Primary link	145.64
3.	Secondary	4683
4.	Tertiary	505.6
5.	Residential	841.42
6.	Unclassified	101.9
7.	Service	101.93
8.	Track	92.87

land, and forest classes are the most affected with 1.531 km^2, 0.345 km^2 and 0.332 km^2 inundation area extent, respectively. About half of the inundated area is irrigated land.

Table 7 shows different road types which were inundated in the study area. The road was classified into eight classes. The results show that secondary link is the most affected road type with 4683 m of road length. The residential, track and service road types are also affected with inundated length of 841.42 m, 92.87 m and 101.93 m respectively.

To determine the variation in flood extent due to different input data, the inundation area map for the uncorrected DEM and corrected DEM are overlaid or intersected with each other and are shown in Fig. 12. Most of the inundated area (2.743 km^2) was simulated by using both the corrected and uncorrected DEMs (the flood extents match). The inundation area which was simulated only by using the uncorrected DEM and corrected DEM is 0.002 km^2 and 0.127 km^2 respectively. This shows that the choice between the raw or corrected DEM has only a small impact on model results in flood extent terms.

4. Conclusion

This study contributes to the limited literature on the value of citizen science data for characterizing and simulating floods using a hydrodynamic flood model. A key limitation of the citizen science method used was the inability to capture floods occurring in the evening and nighttime. Nevertheless, the citizen science data was found adequate to specify the upstream boundary condition and provide data for evaluating the performance of the model for different data sets. The data also enables us to evaluate the model sensitivity to input data including corrected and uncorrected versions of the DEM, with and without incorporating tributary information, and the hydraulic roughness parameter.

DEM correction using 15 field-collected river channel cross-sections was found to substantially improve the accuracy of the simulated water level. Further, the sensitivity analysis indicated that (i) monitoring the water level of only the larger of the two minor tributaries is adequate enough for simulation of the flood level, (ii) the simulated water level is affected more by the Manning's roughness coefficient of the river channel than that of the floodplain, and (iii) the downstream extent of the model domain should be determined based on sensitivity analysis of the downstream boundary condition effect.

The study is conducted in the kind of data scarce environment that prevails in most lower- and middle-income countries. The scarcity of data led us to rely on citizen science data to evaluate model sensitivity. Citizen scientists were not able to record nighttime water level hydrographs with the measurement technique we adopted. Future studies can explore appropriate techniques that enable citizen scientists to record nighttime hydrographs.

Our study showed that data gaps in flood modeling can be filled by engaging citizen scientists for a relatively short period of time. However, additional benefits can be obtained by sustaining the engagement of citizen scientists for a longer term. Therefore, we suggest future studies to explore mechanisms to sustain engagement of citizen scientists in flood monitoring, and also explore ways of engaging them beyond flood hazard, e.g. knowledge co-production to study flood exposure and vulnerability. Finally, we recommend future studies consider different sources of error in order to improve model performance.

Declaration of competing interest

The authors have no conflict of interest to report.

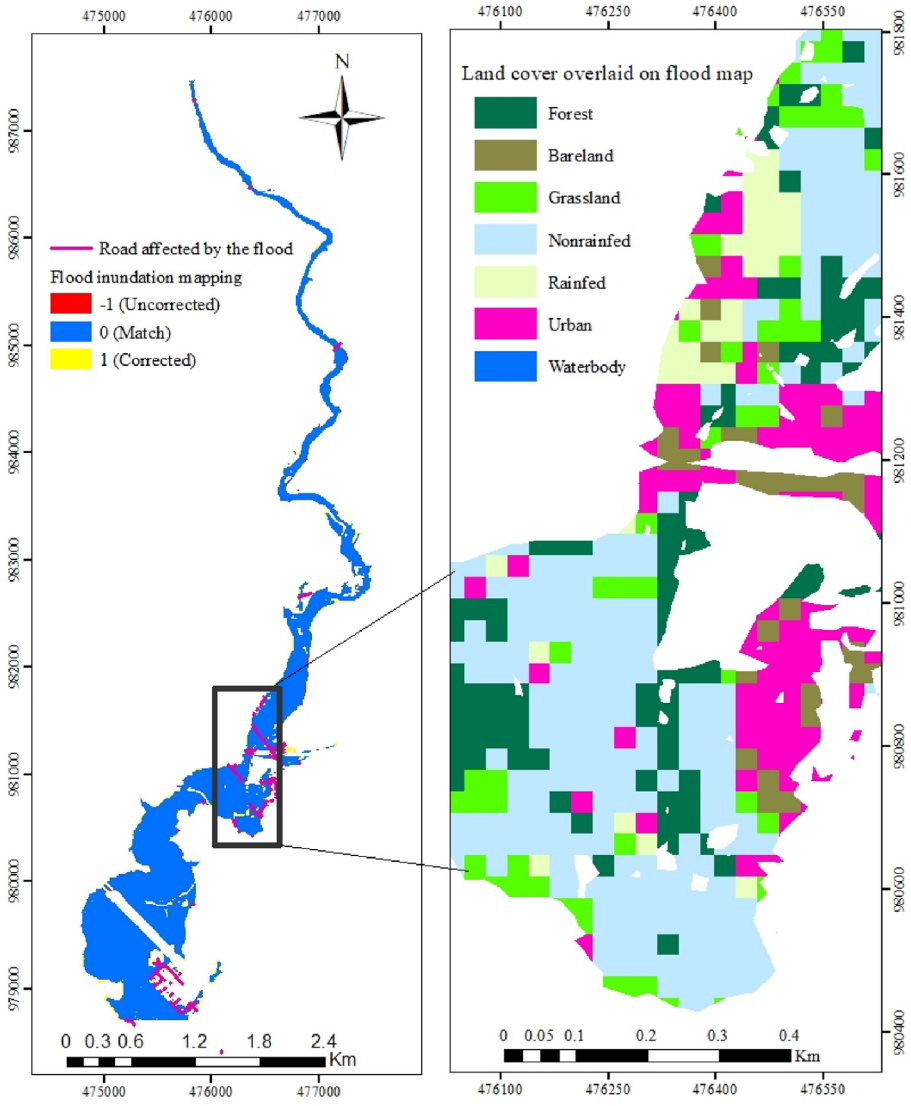

Fig. 12. A. Flood map using uncorrected DEM, corrected DEM and match (both) b. Land cover overlaid on flood map.

Acknowledgment

This research work was supported by Water Security and Sustainable Development Hub funded by the UK Research and Innovation's Global Challenges Research Fund (GCRF), grant number: ES/S008179/1. We would like to thank the Africa Center of Excellence for Water Management (ACEWM) for supporting the study.

References

Aceves-bueno, E., Adeleye, A.S., Feraud, M., Huang, Y., Tao, M., Yang, Y., Anderson, S.E., 2017. Accuracy Citiz. Sci. Data : Quant. Rev. 98 (4), 278–290. https://doi.org/10.1002/bes2.1336.

Arcement, G.J., Schneider, V.R., 1989. Guide for selecting Manning's roughness coefficients for natural channels and flood plains. Anaesthesist 42 (6), 44. Report No. FHWA-TS-84-204.

Asfaw, F., 2007. Modeling on Akaki River Liquid Waste Disposal and Base Flow Separation. Addis Ababa University, 6.

Ashok, V., Sridhar, R.V., Ajey, N.V.U., Patel, K., 2018. Floodplain mapping and management of urban catchment using HEC-RAS : a case study of hyderabad city. J. Inst. Eng.: Series A. https://doi.org/10.1007/s40030-018-0345-0.

Assumpção, T.H., Popescu, I., Jonoski, A., Solomatine, D.P., 2018. Citizen observations contributing to flood modelling: opportunities and challenges. Hydrol. Earth Syst. Sci. 22 (2), 1473–1489. https://doi.org/10.5194/hess-22-1473-2018.

Bannatyne, L.J., Rowntree, K.M., Van Der Waal, B.W., Nyamela, N., 2017. Design and implementation of a citizen technician–based suspended sediment monitoring network: lessons from the tsitsa river catchment, South Africa. WaterSA 43 (3), 365–377. https://doi.org/10.4314/wsa.v43i3.01.

Bekele, T.W., Haile, A.T, Trigg, M.A., Walsh, C.L., 2022. Evaluating a new method of remote sensing for fl ood mapping in the urban and peri-urban areas : applied to Addis Ababa and the Akaki catchment in Ethiopia. Nat. Hazards Res. 2 (2), 97–110. https://doi.org/10.1016/j.nhres.2022.03.001.

Brunner, G.W., 2016. HEC-RAS river analysis system hydraulic reference manual version 5.0. In: *Hydrologic Engineering Center* (Issue February). U.S. Army Corps of Engineers Institute for Water Resources HydrologicHydrologic Engineering Center 609 Second Street, Davis, CA, 95616, 530.

Chow, V. Te, 1959. Open Channel Hydraulics. McGraw-Hill Book Co., New York, p. 680. https://doi.org/10.1016/B978-0-12-821770-2.00022-1.

Dasgupta, A., Grimaldi, S., Ramsankaran, R., Pauwels, V.R.N., Walker, J.P., 2022. A simple framework for calibrating hydraulic flood inundation models using Crowd-sourced water levels. J. Hydrol. 614, 128467. https://doi.org/10.1016/j.jhydrol.2022.128467.

Ethiopia Roads Authority, 2013. Hydrology. In: Drainage Design Manual, pp. 5–61.

Ezzine, A., Saidi, S., Hermassi, T., Kammessi, I., Darragi, F., Rajhi, H., 2020. The Egyptian journal of remote sensing and space sciences flood mapping using hydraulic modeling and sentinel-1 image : case study of medjerda basin , northern Tunisia. Egyp. J. Rem. Sen. Space Sci. xxxx, 1–8. https://doi.org/10.1016/j.ejrs.2020.03.001.

Fava, M.C., Abe, N., Restrepo-Estrada, C., Kimura, B.Y.L., Mendiondo, E.M., 2019. Flood modelling using synthesised citizen science urban streamflow observations. J. Flood Risk Manag. 12 (October 2017), 1–13. https://doi.org/10.1111/jfr3.12498.

Ferreira, D.M., Fernandes, C.V.S., Kaviski, E., Bleninger, T., 2021. Calibration of river hydrodynamic models: analysis from the dynamic component in roughness coefficients. J. Hydrol. 598 (August 2020). https://doi.org/10.1016/j.jhydrol.2021.126136.

Ferri, M., Wehn, U., See, L., Monego, M., Fritz, S., 2020. The value of citizen science for flood risk reduction: cost-benefit analysis of a citizen observatory in the Brenta-

Bacchiglione catchment. Hydrol. Earth Syst. Sci. 24 (12), 5781–5798. https://doi.org/10.5194/hess-24-5781-2020.

Geravand, F., Hosseini, S.M., Ataie-Ashtiani, B., 2020. Influence of river cross-section data resolution on flood inundation modeling: case study of Kashkan river basin in western Iran. J. Hydrol. 584 (December 2019), 124743. https://doi.org/10.1016/j.jhydrol.2020.124743.

Haile, A.T., Rientjes, T.H.M., 2007. Uncertainty issues in hydrodynamic flood modeling. In: Proceedings of the 5th International Symposium on Spatial Data Quality SDQ 2007, Modelling Qualities in Space and TimeITC. Enschede, The Netherlands.

Kane, S., Sambou, S., Leye, I., Diedhiou, R., Tamba, S., Cisse, M.T., Ndione, D.M., Sane, M.L., 2017. Modeling of unsteady flow through junction in rectangular channels: impact of model junction in the downstream channel hydrograph. Comput. Water Energy Environ. Eng. 6 (3), 304–319. https://doi.org/10.4236/cweee.2017.63020.

Lamichhane, N., Sharma, S., 2018. Effect of input data in hydraulic modeling for flood warning systems. Hydrol. Sci. J. 63 (6), 938–956. https://doi.org/10.1080/02626667.2018.1464166.

Lee, J., Kim, J., Jang, W.S., Lim, K.J., Engel, B.A., 2018. Assessment of baseflow estimates considering recession characteristics in SWAT. Water (Switzerland) 10 (4), 1–14. https://doi.org/10.3390/w10040371.

Loftis, J.D., Mitchell, M., Schatt, D., Forrest, D.R., Wang, H.V., Mayfield, D., Stiles, W.A., 2019. Validating an Operational Flood Forecast Model Using Citizen Science in Hampton Roads. VA, USA.

Montargil, F., Santos, V., 2017. Citizen observatories: concept, opportunities and communication with citizens in the first EU experiences. In: Paulin, A.A., Anthopoulos, L.G., Reddick, C.G. (Eds.), Beyond Bureaucracy: towards Sustainable Governance Informatisation. Springer International Publishing, pp. 167–184. https://doi.org/10.1007/978-3-319-54142-6_11.

Muthusamy, M., Casado, M.R., Butler, D., Leinster, P., 2021. Understanding the effects of Digital Elevation Model resolution in urban fluvial flood modelling. J. Hydrol. 596 (February). https://doi.org/10.1016/j.jhydrol.2021.126088.

Natarajan, S., Radhakrishnan, N., 2020. An integrated hydrologic and hydraulic flood modeling study for a medium-sized ungauged urban catchment area : a case study of tiruchirappalli city using HEC-HMS and HEC-RAS. J. Inst. Eng.: Series A. https://doi.org/10.1007/s40030-019-00427-2.

Pandeya, B., Uprety, M., Paul, J.D., Sharma, R.R., Dugar, S., Buytaert, W., 2021. Mitigating flood risk using low-cost sensors and citizen science: a proof-of-concept study from western Nepal. J. Flood Risk Manag. 14 (1), 1–13. https://doi.org/10.1111/jfr3.12675.

Paul, J.D., Cieslik, K., Sah, N., Shakya, P., Parajuli, B.P., Paudel, S., Dewulf, A., Buytaert, W., Paul, J.D., 2020. Applying Citizen Science for Sustainable Development : Rainfall Monitoring in Western Nepal, 2, pp. 1–12. https://doi.org/10.3389/frwa.2020.581375. December.

Rollason, E., Bracken, L.J., Hardy, R.J., Large, A.R.G., 2018. The importance of volunteered geographic information for the validation of flood inundation models. J. Hydrol. 562 (November 2017), 267–280. https://doi.org/10.1016/j.jhydrol.2018.05.002.

Ruiz-bellet, J.L., Castelltort, X., Balasch, J.C., Tuset, J., 2017. Uncertainty of the Peak Flow Reconstruction of the 1907 Flood in the Ebro River in Xerta (NE Iberian Peninsula), 545, pp. 339–354. https://doi.org/10.1016/j.jhydrol.2016.12.041.

Sanyal, J., 2017. Uncertainty in levee heights and its effect on the spatial pattern of flood hazard in a floodplain in a floodplain. Hydrol. Sci. J. 62 (9), 1483–1498. https://doi.org/10.1080/02626667.2017.1334887.

Sermet, Y., Villanueva, P., Sit, M.A., Demir, I., 2020. Crowdsourced approaches for stage measurements at ungauged locations using smartphones. Hydrol. Sci. J. 65 (5), 813–822. https://doi.org/10.1080/02626667.2019.1659508.

Starkey, E., Parkin, G., Birkinshaw, S., Large, A., Quinn, P., Gibson, C., 2017. Demonstrating the value of community-based (‘ citizen science ’) observations for catchment modelling and characterisation. J. Hydrol. 548, 801–817. https://doi.org/10.1016/j.jhydrol.2017.03.019.

Strobl, B., Etter, S., Meerveld, I. Van, Seibert, J., Strobl, B., Etter, S., 2019. Accuracy of crowdsourced streamflow and stream level class estimates Accuracy of crowdsourced streamflow and stream level class estimates. Hydrol. Sci. J. 0 (0), 1–19. https://doi.org/10.1080/02626667.2019.1578966.

Sy, B., Frischknecht, C., Dao, H., Consuegra, D., Giuliani, G., 2019. Flood hazard assessment and the role of citizen science. J. Flood Risk Manag. 12. https://doi.org/10.1111/jfr3.12519.

Tedla, H.Z., Haile, A.T., Walker, D.W., Melesse, A.M., 2022. Evaluation of factors affecting the quality of citizen science rainfall data in Akaki catchment, Addis Ababa, Ethiopia. J. Hydrol. 612, 128284. https://doi.org/10.1016/j.jhydrol.2022.128284.

Wolff, E., French, M., Ilhamsyah, N., Sawailau, M.J., Ramírez-lovering, D., 2021. Collaborating with communities: citizen science flood monitoring in urban informal settlements. Urban. Plann. 6 (4), 351–364. https://doi.org/10.17645/up.v6i4.4648.

Worako, A.W., 2016. Land use land cover change detection by using remote sensing data in Akaki River basin. Int. J. Environ. Agri. Biotechnol. 1 (Issue-1).